

Sensitivity studies for the main r process: β -decay rates

M. Mumpower, J. Cass, G. Passucci, R. Surman, and A. Aprahamian

Citation: *AIP Advances* **4**, 041009 (2014); doi: 10.1063/1.4867192

View online: <http://dx.doi.org/10.1063/1.4867192>

View Table of Contents: <http://scitation.aip.org/content/aip/journal/adva/4/4?ver=pdfcov>

Published by the *AIP Publishing*

Articles you may be interested in

[Sensitivity studies for the weak r process: neutron capture rates](#)

AIP Advances **4**, 041008 (2014); 10.1063/1.4867191

[First-forbidden transitions in N=126 isotones and r-process nucleosynthesis](#)

AIP Conf. Proc. **1484**, 363 (2012); 10.1063/1.4763421

[Gamow-Teller Transitions Studied in \(\$^3\text{He}\$, t\) Reaction and Analogous \$\beta\$ decay](#)

AIP Conf. Proc. **1265**, 148 (2010); 10.1063/1.3480153

[Relativistic QRPA Calculation of \$\beta\$ Decay Rates of rprocess Nuclei](#)

AIP Conf. Proc. **1165**, 433 (2009); 10.1063/1.3232144

[\$\beta\$ -decay rates—The semi-gross theory—](#)

AIP Conf. Proc. **425**, 495 (1998); 10.1063/1.55191

An advertisement for AIP's journal. It features a row of computer monitors in a library or office setting, each displaying the journal's cover. The cover art shows a colorful, swirling pattern. The text 'computing' is written in a stylized font, with 'SCIENCE & ENGINEERING' underneath. Below the monitors, the text reads 'AIP'S JOURNAL OF COMPUTATIONAL TOOLS AND METHODS. AVAILABLE AT MOST LIBRARIES.'

computing
SCIENCE & ENGINEERING

AIP'S JOURNAL OF COMPUTATIONAL TOOLS AND METHODS.
AVAILABLE AT MOST LIBRARIES.

Sensitivity studies for the main r process: β -decay rates

M. Mumpower,¹ J. Cass,¹ G. Passucci,¹ R. Surman,² and A. Aprahamian¹

¹*Department of Physics, University of Notre Dame, Notre Dame, Indiana 46556, USA*

²*Department of Physics & Astronomy, Union College, Schenectady, New York 12308, USA*

(Received 9 December 2013; accepted 23 December 2013; published online 26 February 2014)

The pattern of isotopic abundances produced in rapid neutron capture, or r -process, nucleosynthesis is sensitive to the nuclear physics properties of thousands of unstable neutron-rich nuclear species that participate in the process. It has long been recognized that some of the most influential pieces of nuclear data for r -process simulations are β -decay lifetimes. In light of experimental advances that have pushed measurement capabilities closer to the classic r -process path, we revisit the role of individual β -decay rates in the r process. We perform β -decay rate sensitivity studies for a main ($A > 120$) r process in a range of potential astrophysical scenarios. We study the influence of individual rates during (n, γ) - (γ, n) equilibrium and during the post-equilibrium phase where material moves back toward stability. We confirm the widely accepted view that the most important lifetimes are those of nuclei along the r -process path for each astrophysical scenario considered. However, we find in addition that individual β -decay rates continue to shape the final abundance pattern through the post-equilibrium phase, for as long as neutron capture competes with β decay. Many of the lifetimes important for this phase of the r process are within current or near future experimental reach. © 2014 Author(s). All article content, except where otherwise noted, is licensed under a Creative Commons Attribution 3.0 Unported License. [<http://dx.doi.org/10.1063/1.4867192>]

I. INTRODUCTION

The continuous build up of heavier nuclei via neutron captures and β decays during astrophysical events occurs primarily on short or long timescales in the r and s processes of nucleosynthesis.^{1,2} The slow neutron capture process (s process) proceeds over timescales of millions of years in AGB stars ultimately ending with the production of ²⁰⁹Bi.³ While the nuclear physics properties and astrophysical conditions of the s process are well established these issues still remain open for the rapid neutron capture process (r process). Many candidate sites for the r process have been proposed including promising environments in supernova and the merger of neutron stars. However, each of these sites suffer from their own unresolved problems; see Refs. 4 and 5 and references therein.

From the perspective of nuclear physics, much of the difficulty of constraining the astrophysical site for the r process comes from the challenge and sheer number of measurements that must be performed on thousands of short-lived neutron-rich nuclei far from stability that may participate in this process. For instance, neutron captures in the r process are believed to first exceed and then compete with β decays allowing for the set of most abundant isotopes or “path” to potentially push out to the neutron dripline. Thus β -decay lifetimes of these nuclei are critical inputs for the r process because they not only set the timescale for heavy element production if (n, γ) - (γ, n) equilibrium occurs but also help to shape the final pattern as the path moves back to stability.^{6,7}

To date there have been many studies of β -decay rates most of which have focused on so-called ‘waiting point’ nuclei. Waiting point nuclei are those that accrue substantial mass fraction for a given time relative to the timescale of the nucleosynthesis process at hand. Ref. 8 studied the β decays of waiting point nuclei along the $N = 126$ isotone noting a shift in the $A = 195$ peak when first-forbidden transitions were taken into account. Inclusion of the latest measurements of β -decay half-lives is



also important. Using recent measurements from RIKEN Ref. 9 demonstrated an enhancement of abundances in the region below the $A = 130$ peak which shifted the pattern closer to solar.

In this work we study the influence of individual β -decay rates across the chart of nuclides in the context of a main r process which produces nuclear flow out to the third ($A = 195$) abundance peak. Section II covers the details of our reaction network calculations and section III covers our assumptions about astrophysical conditions. In section IV we provide an overview of our sensitivity study calculations. The results of our sensitivity studies are discussed in sections V–VII.

II. NUCLEAR NETWORK CALCULATION

In the majority of astrophysical scenarios considered, the r process is a primary process in which element synthesis begins from initially hot ($T > 10$ GK) material composed of free neutrons and protons. A full r -process calculation therefore involves a network of differential equations for every nuclear species and all of the strong, electromagnetic, and weak interactions that connect them. However, the rapid neutron capturing that characterizes the r process and produces the heaviest nuclei $A > 120$ does not begin in earnest until the temperature has dropped to $T \sim 2$ GK and the charged particle interactions have largely ceased. Thus the remaining nuclear reactions important for the r process include only neutron capture, photodissociation, β decay, and β -delayed neutron emission (and possibly fission). Therefore for each nuclear species (Z, A) the following equation governs its change in abundance:

$$\begin{aligned} \dot{Y}(Z, A) = & Y(Z, A - 1)\lambda_n^{Z, A-1} + Y(Z, A + 1)\lambda_\gamma^{Z, A+1} \\ & - Y(Z, A)(\lambda_n^{Z, A} + \lambda_\gamma^{Z, A} + \lambda_\beta^{Z, A} + \lambda_{\beta n}^{Z, A} + \lambda_{\beta 2n}^{Z, A} + \lambda_{\beta 3n}^{Z, A}) \\ & + Y(Z - 1, A)\lambda_\beta^{Z-1, A} + Y(Z - 1, A + 1)\lambda_{\beta n}^{Z-1, A+1} \\ & + Y(Z - 1, A + 2)\lambda_{\beta 2n}^{Z-1, A+2} + Y(Z - 1, A + 3)\lambda_{\beta 3n}^{Z-1, A+3}, \end{aligned} \quad (1)$$

where $Y(Z, A)$ is the abundance of nucleus (Z, A), λ_n the neutron capture rate, λ_γ the photodissociation rate, λ_β the β -decay rate, and $\lambda_{\beta xn}$ the rate for β -decay followed by emission of x neutrons. It is important to note that the neutron number density n_n , though not written out explicitly above, determines the neutron capture rate, $\lambda_n = n_n \langle \sigma v \rangle$ (where $\langle \sigma v \rangle$ is the thermally averaged (n, γ) reaction rate), and the photodissociation rate, through detailed balance. The coupled set of 3000 or so of these equations, one for each nuclear species, forms the r -process network. They are solved given initial inputs of the astrophysical conditions (temperature, density, etc. as a function of time) and the relevant nuclear physics properties (masses, β -decay lifetimes and β -delayed neutron emission probabilities, neutron capture rates, etc.). Here we use a nuclear network code from Ref. 10. The nuclear physics input includes neutron capture rates from Ref. 11 and nuclear masses from Refs. 12 and 13. We consider two compilations of β -decay rates: a purely theoretical set of rates from Ref. 14, and a combined set where the experimental rates from Ref. 15 are included where available. Fission is treated as in Ref. 16.

While the details of the r process will vary depending on the astrophysical conditions, a typical simulation will proceed in three phases. The first phase is the (n, γ) - (γ, n) equilibrium phase, in which the temperature and neutron number densities are sufficiently high such that an equilibrium is established between captures and photodissociations. In this phase, the abundances along an isotopic chain are determined by a Saha equation:

$$I_{00} = \frac{Y(Z, A + 1)}{Y(Z, A)} = \frac{G(Z, A + 1)}{2G(Z, A)} \left(\frac{2\pi \hbar^2 N_A}{m_n kT} \right)^{3/2} n_n \quad (2)$$

$$\times \exp \left[\frac{S_n(Z, A + 1)}{kT} \right] \quad (3)$$

where the G s are the partition functions, m_n is the nucleon mass, and S_n are the one-neutron separation energies. Thus, the abundances along an isotopic chain are determined from the nuclear masses.

The relative abundances of the different isotopic chains are set by the β -decay lifetimes of the most populated nuclei along each chain. This chain of most populated nuclei is called the r -process path, and in steady state the abundances along it are characterized by the steady β flow condition:

$$Y(Z, A_{\text{path}})\lambda_{\beta}(Z, A_{\text{path}}) = \text{constant}. \quad (4)$$

Eventually, either the temperature drops or the supply of free neutrons is exhausted and (n, γ) - (γ, n) equilibrium begins to fail. In this second phase of the r process—the freezeout phase—the shapes of the main peaks are finalized¹⁰ and the rare earth peak forms.^{7,17} During this phase individual neutron capture rates, photodissociation rates, β -decay rates, and β -delayed neutron emission probabilities can all play a role in shaping the final r -process abundance pattern. The final phase of the r -process is the decay back to stability, which begins in earnest once the timescale for neutron capture becomes much longer than the β -decay timescale. The abundance pattern as a function of mass number A is largely set by this time, with fine details determined by the relevant β -delayed neutron emission probabilities.

From this general picture, we expect the individual β -decay rates of nuclei along the r -process path in the equilibrium phase to be of primary importance in determining the r -process abundances. However, β -decay rates will continue to shape the r -process pattern throughout the freezeout phase and as the material moves toward stability. Exactly which lifetimes are most important will thus be highly dependent on the astrophysical scenario.

III. ASTROPHYSICAL SCENARIOS

We begin our sensitivity studies with baseline simulations chosen from a range of potential astrophysical scenarios that produce a main ($A > 120$) r process. The scenarios fall into two broad categories—mildly heated, very neutron-rich neutron star merger ejecta, and hot astrophysical winds, such as the core-collapse supernova neutrino-driven wind or winds from gamma-ray burst-type black hole accretion disks. Within the latter category we choose trajectories which produce either a classic hot r -process or a cold r -process.¹⁸

A classic hot wind main r -process is characterized by an (n, γ) - (γ, n) equilibrium phase during which the r -process peaks at $A \sim 130$ and $A \sim 195$ are produced, followed by a freezeout phase, as described above, that is triggered by the depletion of free neutrons. For the hot wind r processes considered here, we use the wind parameterization from Ref. 19 as implemented in Ref. 20, with entropies $s/k = 50 - 200$, dynamical timescale $\tau_{\text{dyn}} = 80$ ms, and initial electron fractions $Y_e = 0.25 - 0.35$. The final abundance pattern produced by an example hot wind trajectory is shown in Fig. 1.

The temperatures and densities in a realistic wind can drop more rapidly than in the classic hot parameterized wind described above. In this type of scenario, called a cold r -process,¹⁸ (n, γ) - (γ, n) equilibrium is established only briefly, since photodissociations become negligible once the temperature drops below ~ 0.1 GK. The r process can proceed to build the heavy peaks, however, as long as the free neutron abundance remains high. Without photodissociations to push material back towards stability, the r -process path moves toward the neutron drip line, and a new equilibrium can be established between neutron captures and β decays. For the cold r -process winds, we implement the wind parameterization of Ref. 23 with entropies $s/k = 50 - 300$, dynamical timescales $\tau_{\text{dyn}} = 20 - 200$ ms, and initial electron fractions $Y_e = 0.25 - 0.4$. We additionally include three trajectories from the neutrino-driven wind simulations of Ref. 21, where we artificially reduce the electron fractions to $Y_e = 0.31 - 0.33$ to produce a main r process. The final abundance pattern from the 15 solar mass case with $Y_e = 0.33$ is shown in Fig. 1.

The final scenario we consider is the ejection of mildly heated, very neutron-rich material from the tidal tails of a neutron star merger. We start with a trajectory from a merger simulation by A. Bauswain and H.-Th. Janka, similar to those from Ref. 24. We then extrapolate it out to low temperatures, keeping the entropy constant, as validated by recent merger simulations followed to late times.²⁵ The resulting r process proceeds in (n, γ) - (γ, n) equilibrium as in the classic hot r process, but here freezeout is prompted by the drop in temperature and density rather than an

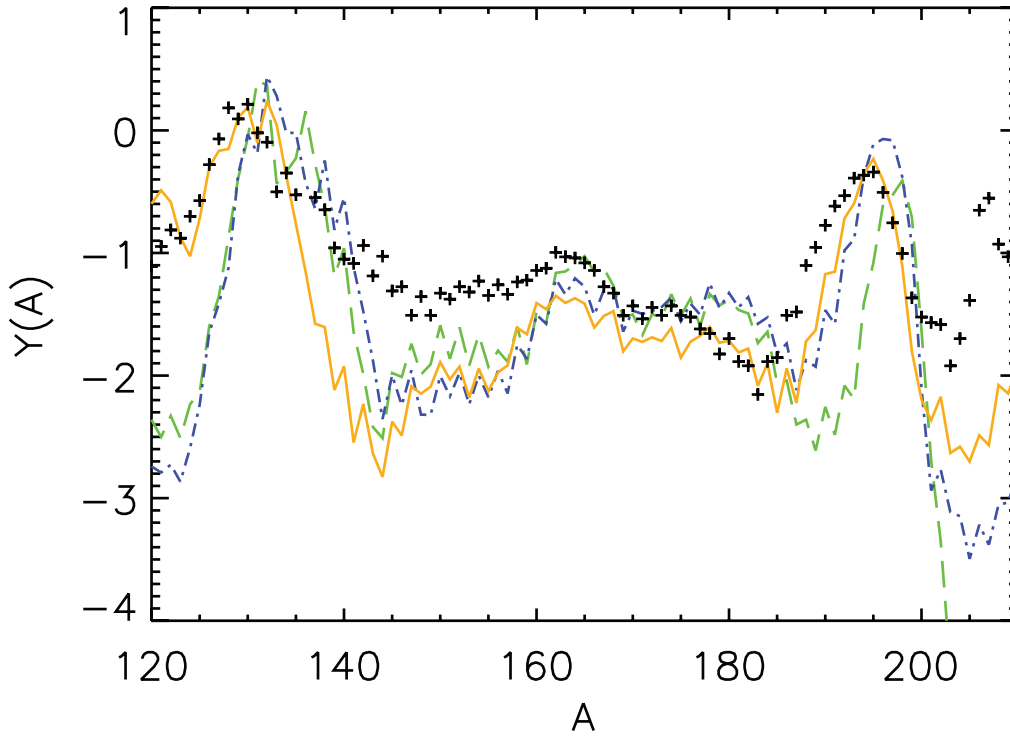


FIG. 1. Final abundances $Y(A)$ versus mass number A for three sample astrophysical trajectories: a hot wind r -process parameterized as in Ref. 19 and 20 with entropy $s/k = 100$, dynamical timescale $\tau_{\text{dyn}} = 80$ ms, and initial electron fraction $Y_e = 0.25$ (dashed green line), a cold wind r process from Ref. 21 (dot-dashed blue line), and a neutron star merger r process as described in the text (solid gold line). All three abundance patterns are scaled to the solar pattern from Ref. 22 (crosses).

exhaustion of free neutrons as in the hot r -process case. Neutrons are in fact so plentiful that fission recycling occurs. This abundance pattern is shown in Fig. 1 as well.

IV. SENSITIVITY STUDY

Once our set of baseline astrophysical trajectories are chosen, we run a β -decay sensitivity study for each. Each sensitivity study consists of over 4000 repetitions of the baseline simulation, where for each repetition a single β -decay rate is either increased or decreased by a consistent factor. To guide our choice of a reasonable rate variation factor, we examine a comparison between experiment and theory as shown in Fig. 2. Since the discrepancies between theory and experiment can be an order of magnitude or more, we choose a factor of ten for our rate variations. Finally we compare the final abundance patterns produced with the β -decay rate variations to the baseline pattern using the sensitivity measure F , similar to Refs. 26–28:

$$F = 100 \times \left\{ \sum_A |AY_{\text{baseline}}(A) - AY_{\text{increase}}(A)| + \sum_A |AY_{\text{baseline}}(A) - AY_{\text{decrease}}(A)| \right\} / 2 \quad (5)$$

where $Y_{\text{baseline}}(A)$ are the final baseline abundances, and $Y_{\text{increase}}(A)$ and $Y_{\text{decrease}}(A)$ are final abundances of the simulations where a single β -decay rate is increased or decreased, respectively. Sensitivity measures for the three example trajectories from Fig. 1 are found in Fig. 3 and Table I and described in the sections below. Additional sample results and analysis from this large set of sensitivity studies can be found in Refs. 28–30.

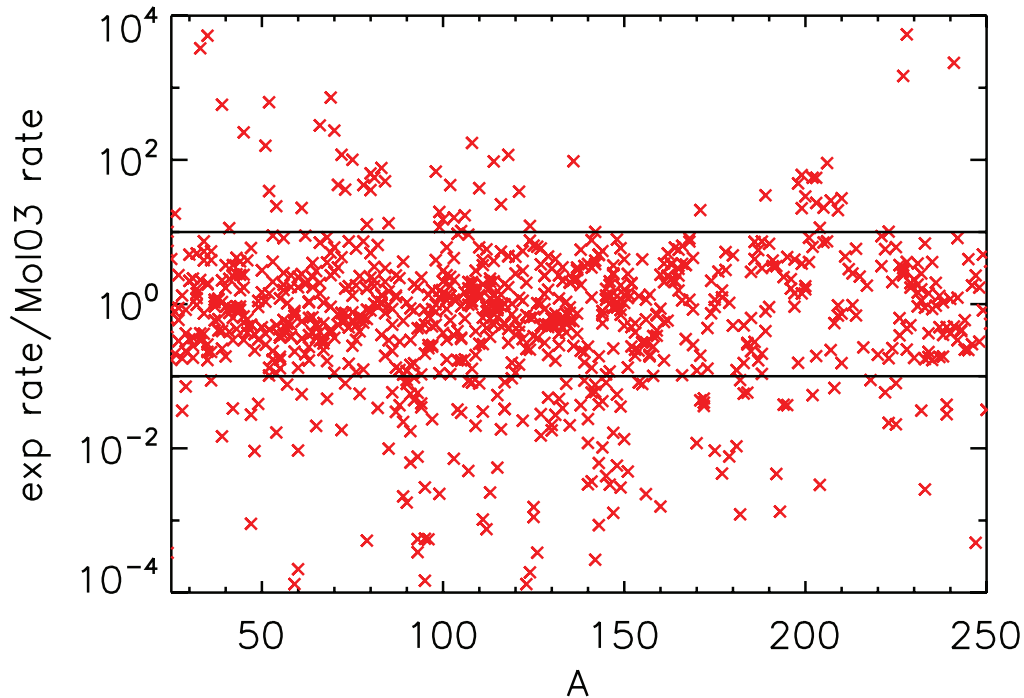


FIG. 2. The ratios of the experimental decay rates from Ref. 15 to the theoretical decay rates from Ref. 14 (red points), for nuclei where the experimental lifetimes are available. The largest deviations are found for nuclei farthest from stability (see also Fig. 4 from Ref. 14). We choose a factor of 10 (black lines) for our rate variations.

V. β DECAY IN EQUILIBRIUM

As expected, our sensitivity studies confirm that the most influential β -decay rates are those of nuclei that lie along the r -process path in the equilibrium phase. This is illustrated in Fig. 4, which compares the sensitivity measures F from the hot wind r -process example to the abundances in the equilibrium phase for the same simulation. To confirm that the strong influence of the β -decay rates along the r -process path occurs during the equilibrium phase, we repeat the sensitivity study with the same baseline simulation, now terminated before the end of the equilibrium phase. The results of this equilibrium-only sensitivity study appear in the bottom panel of Fig. 4.

The steady β flow approximation furthermore suggests that the potential impact of the β -decay rate of a nucleus along the path will be roughly in proportion to its abundance during equilibrium. This is tested in Fig. 5 for the three sensitivity studies from Fig. 3. Steady β flow is established in all three cases, even the cold r -process example where (n, γ) - (γ, n) equilibrium holds only very briefly.²⁸ As a result, each simulation is the most sensitive to the β -decay lifetimes of the longest lived and thus most abundant nuclei along the path. Examples of abundance patterns produced when the β -decay rate of one nucleus along the equilibrium r -process path is varied can be found in Ref. 28.

VI. β DECAY IN FREEZEOUT

The equilibrium-only sensitivity study results from Fig. 4 clearly shows that the sensitivity of the r process to the β -decay rates of nuclei along the steady-state r -process path arises during (and is largely limited to) the equilibrium phase. The results also suggest that the sensitivity of the r process to the β -decay rates of nuclei between the r -process path and stability arises principally during the freezeout phase. In all three cases from Fig. 3, we find sensitivity measures F for these nuclei that are significant but not as large as those for nuclei along the equilibrium r -process path. This is because the path is moving toward stability during the freezeout phase and steady β flow no longer obtains.

The drop in sensitivity measures along the r -process path during the freezeout phase in the hot r -process example simulation is shown in Fig. 6. During the equilibrium phase, the timescales for

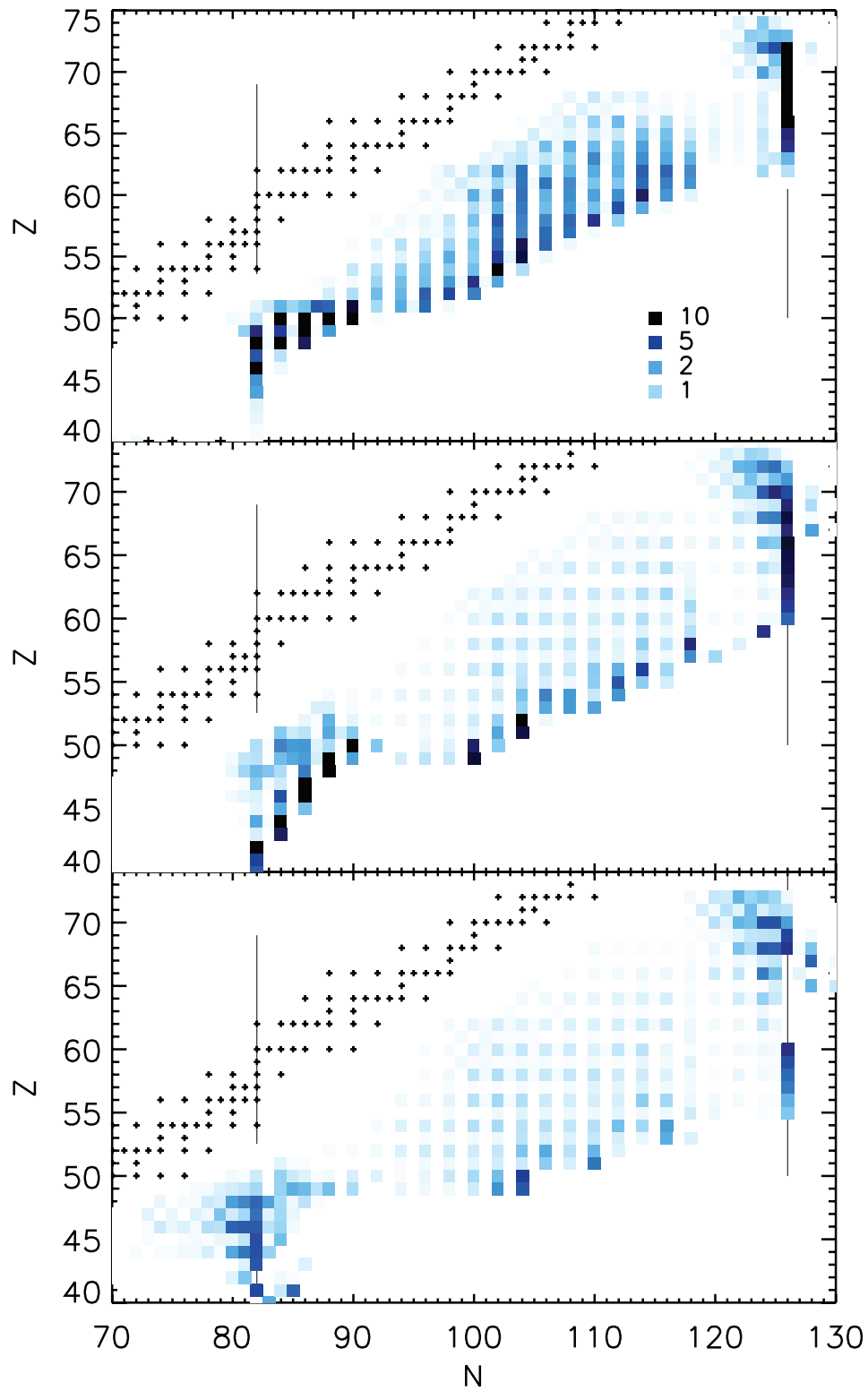


FIG. 3. Shows the average sensitivity measures F (Eqn. (5)) for β -decay sensitivity studies in three example astrophysical scenarios. The F measure color scheme is indicated in the lower right hand corner of the top panel; the darkest squares show nuclei with $F > 10$. The astrophysical trajectories chosen for the baseline simulations are the hot r -process wind (top panel), cold r -process wind (middle panel), and neutron star merger trajectory (bottom panel) from Fig. 1.

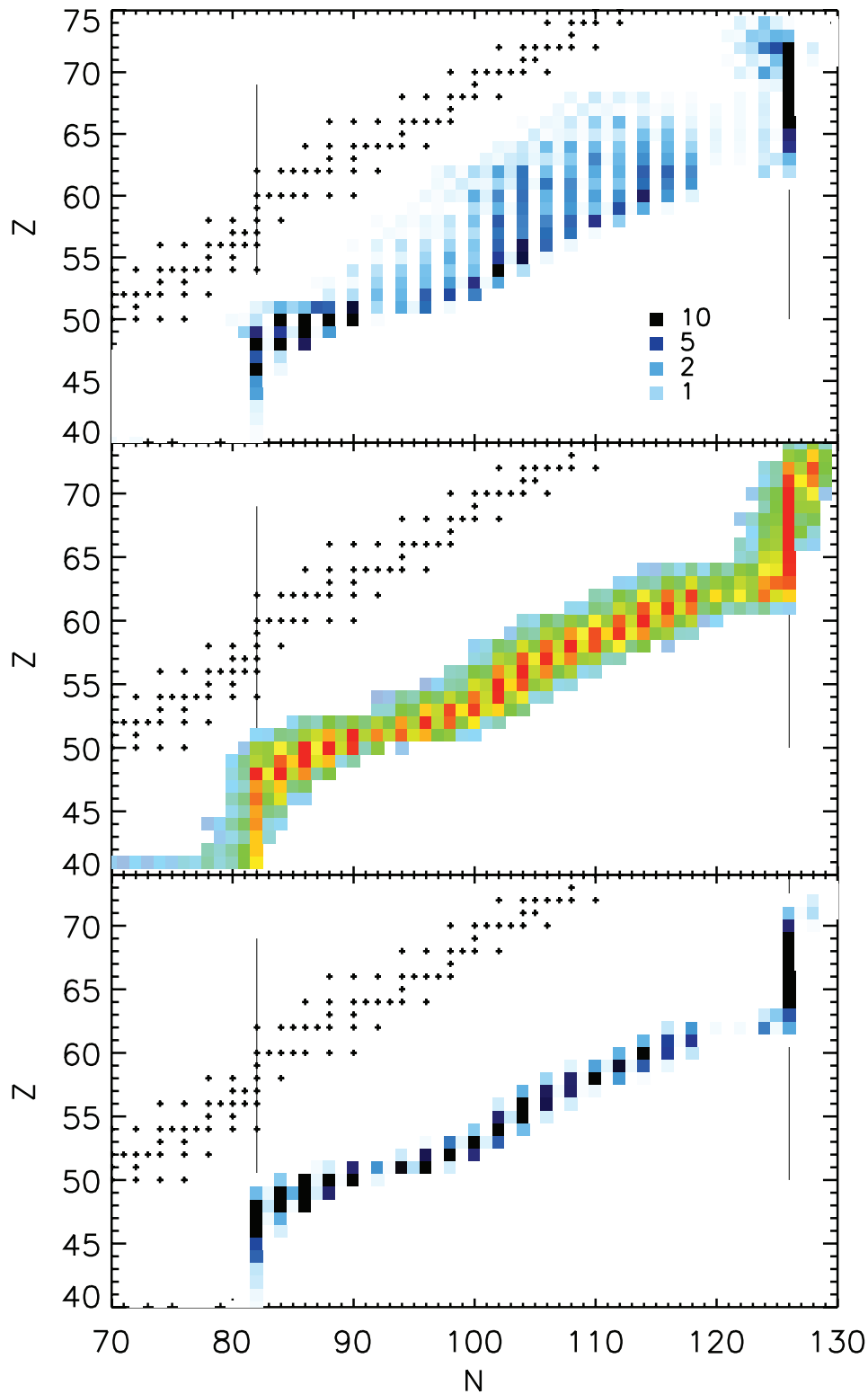


FIG. 4. The top panel is a repeat from Fig. 3 and shows the average sensitivity measure F (Eqn. (5)) for the hot r -process example from Fig. 1. The middle panel shows the abundances in equilibrium on an arbitrary scale for the same simulation, and the bottom panel shows the results of a sensitivity study with the same trajectory that terminates at the end of the equilibrium phase. As expected, the greatest sensitivity measures are found for nuclei along the r -process path.

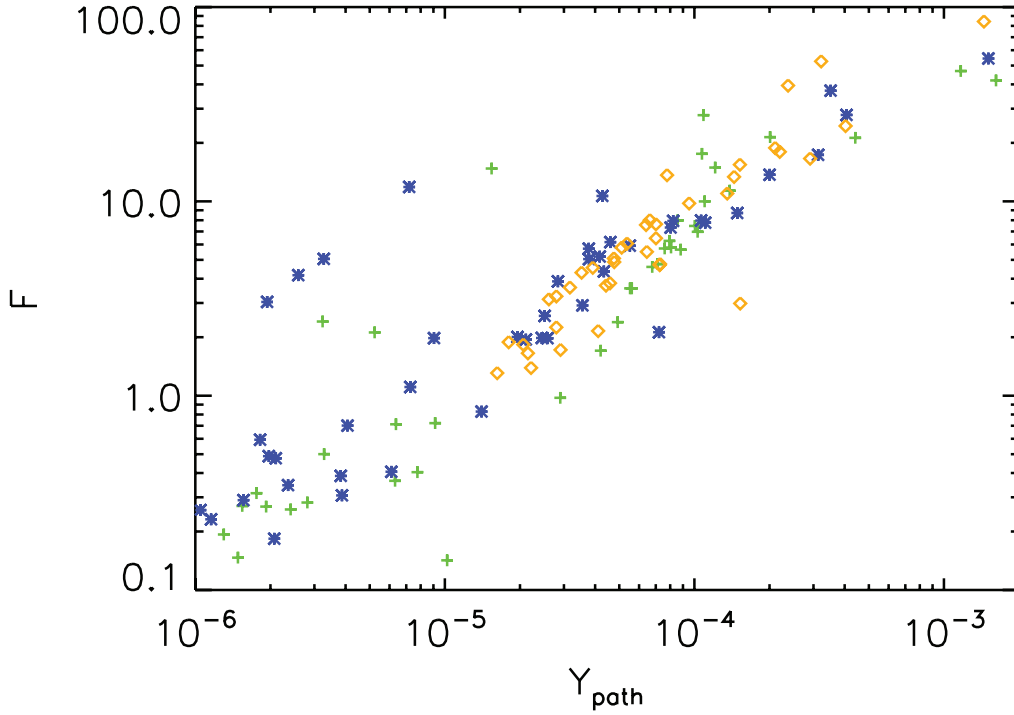


FIG. 5. Sensitivity measures F plotted against the equilibrium abundances Y for nuclei along the r -process path for the hot (green crosses), cold (blue asterisks), and merger (gold diamonds) r -process example simulations from Fig. 1. Note for the cold r process equilibrium refers to the (approximate) equilibrium established between β decays and neutron captures, not the (n, γ) - (γ, n) equilibrium of the other two cases. In all cases the establishment of steady beta flow leads to a roughly proportional relationship between the abundances of nuclei along the equilibrium r -process path and the impact of their β -decay rates.

neutron captures $\tau_{(n, \gamma)}$ and photodissociations $\tau_{(\gamma, n)}$ are much faster than for β decays τ_β , where the timescales are defined as:

$$\tau_{(n, \gamma)} = \frac{\sum Y(Z, A)}{\sum \lambda_{(n, \gamma)}(Z, A)Y(Z, A)} \quad (6)$$

$$\tau_{(\gamma, n)} = \frac{\sum Y(Z, A)}{\sum \lambda_{(\gamma, n)}(Z, A)Y(Z, A)} \quad (7)$$

$$\tau_\beta = \frac{\sum Y(Z, A)}{\sum \lambda_\beta(Z, A)Y(Z, A)} \quad (8)$$

where $Y(Z, A)$ are the abundances and $\lambda_{(n, \gamma)}$, $\lambda_{(\gamma, n)}$, and λ_β are the neutron capture, photodissociation, and β -decay rates, respectively. Fig. 6 shows how the relative timescale ratios $\tau_{(n, \gamma)}/\tau_\beta$ and $\tau_{(\gamma, n)}/\tau_\beta$ evolve during the hot r -process example simulation. During the equilibrium phase, $\tau_{(n, \gamma)} = \tau_{(\gamma, n)} \ll \tau_\beta$ so the ratios $\tau_{(n, \gamma)}/\tau_\beta$ and $\tau_{(\gamma, n)}/\tau_\beta$ are essentially zero. The sensitivities of the r -process to the β -decay rates along the r -process path during this time are very large, and the average F measures obtained along the path exceed 10, also as shown in Fig. 6. At around $t \sim 1$ s, $\tau_{(n, \gamma)}/\tau_\beta$ and $\tau_{(\gamma, n)}/\tau_\beta$ climb and then diverge as (n, γ) - (γ, n) equilibrium fails. While photodissociations quickly drop out of the picture, neutron captures and β decays continue to compete, with $\tau_{(n, \gamma)}/\tau_\beta < 5$, for another second or so. During this phase, the average F measures along the path gradually drop, and eventually become insignificant once $\tau_{(n, \gamma)} \gg \tau_\beta$.

A similar figure for the cold r -process example simulation is shown in Fig. 7. Several differences compared to the hot r -process case are apparent. Even at very early times, the ratios $\tau_{(n, \gamma)}/\tau_\beta$ and $\tau_{(\gamma, n)}/\tau_\beta$ don't quite equal each other; this is because the system falls very quickly out of (n, γ) - (γ, n)

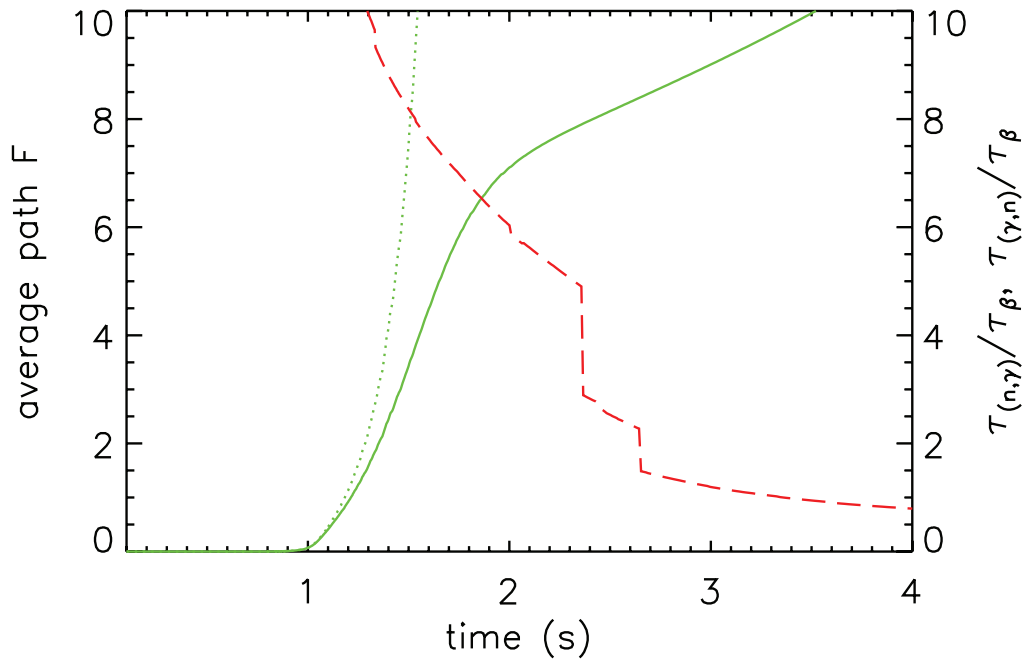


FIG. 6. Average sensitivity measures F (red dashed line) along the r -process path as a function of time in the hot r -process example simulation from Fig. 1. Note the average sensitivity measures along the path exceed 10 for times less than ~ 1.3 s. These are compared to the ratio of the timescales for neutron capture and β decay, $\tau_{(n,\gamma)}/\tau_{\beta}$ (solid line), and the ratio of the timescales for photodissociation and β decay, $\tau_{(\gamma,n)}/\tau_{\beta}$ (dotted line).

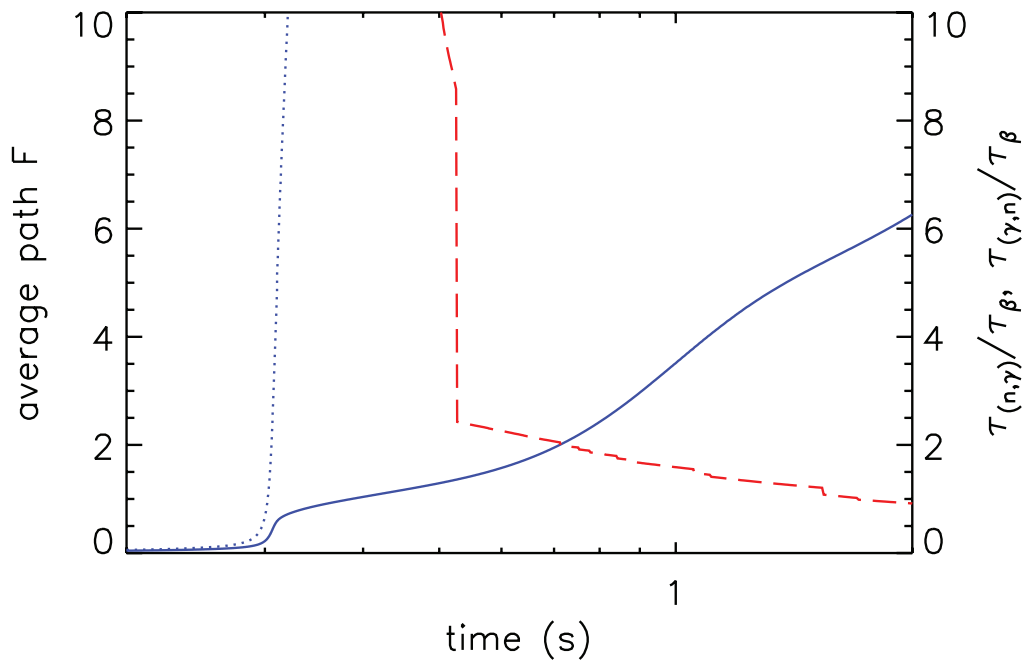


FIG. 7. Average sensitivity measures F (red dashed line) along the r -process path as a function of time in the cold r -process example simulation from Fig. 1. Note the average sensitivity measures along the path exceed 10 for times less than ~ 0.5 s. These are compared to the ratio of the timescales for neutron capture and β decay, $\tau_{(n,\gamma)}/\tau_{\beta}$ (solid line), and the ratio of the timescales for photodissociation and β decay, $\tau_{(\gamma,n)}/\tau_{\beta}$ (dotted line).

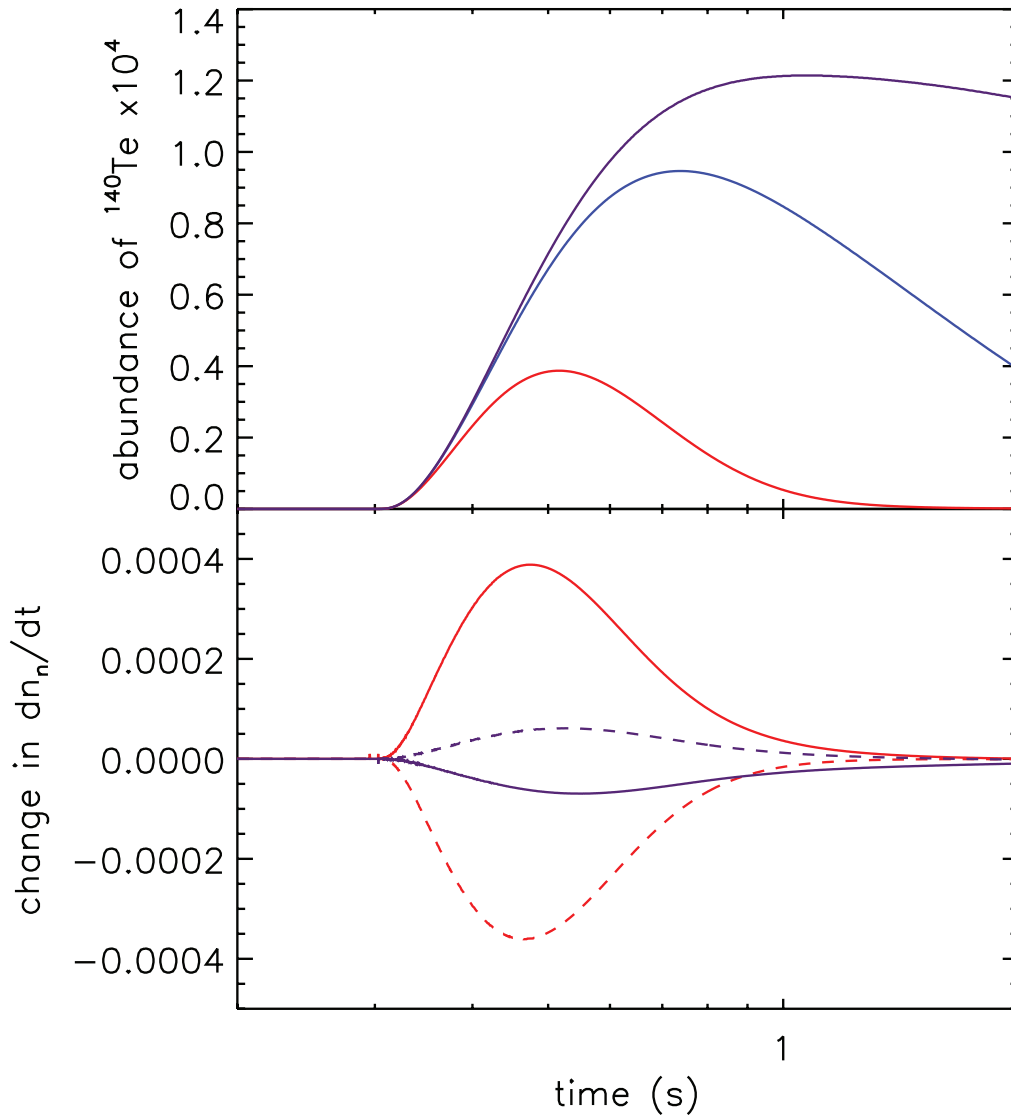


FIG. 8. Top panel shows the abundance of ^{140}Te as a function of time in three simulations of the cold r -process example: the baseline simulation (blue line) and simulations where the β -decay rate of ^{140}Te is either increased (red line) or decreased (purple line) by a factor of 10, as in our sensitivity studies. The bottom panel shows the change in the rate at which neutrons are captured in the $A \sim 130$ region and just above (solid lines) compared to elsewhere in the pattern (dashed lines) for the simulation where the β -decay rate of ^{140}Te is increased (red lines) or decreased (purple lines) by a factor of 10 compared to the baseline simulation.

n) equilibrium, and by $t \sim 0.3$ s photodissociations cease to play a role in the r -process dynamics. Instead, a rough equilibrium is established between neutron captures and β decays for some tenths of seconds, while $\tau_{(n,\gamma)}/\tau_\beta \sim 1$. The average sensitivity measures F along the r -process path remain high through this second equilibrium phase, and drop only after $\tau_{(n,\gamma)}/\tau_\beta > 2$. Here the freezeout phase begins in earnest, and, as in the hot r -process case, the average sensitivity measures F along the r -process path drop markedly as steady β flow no longer obtains. Since the path starts much further from stability where the lifetimes are very short, the path moves rapidly back toward stability during this phase. Thus the potential impact of any one individual rate is less than in the hot r -process case, and the average sensitivity measures F along the path are correspondingly smaller.

During the freezeout phase, a change to an individual β -decay rate can modify the nuclear flow as material moves toward stability. Generally this will produce a small local change to the

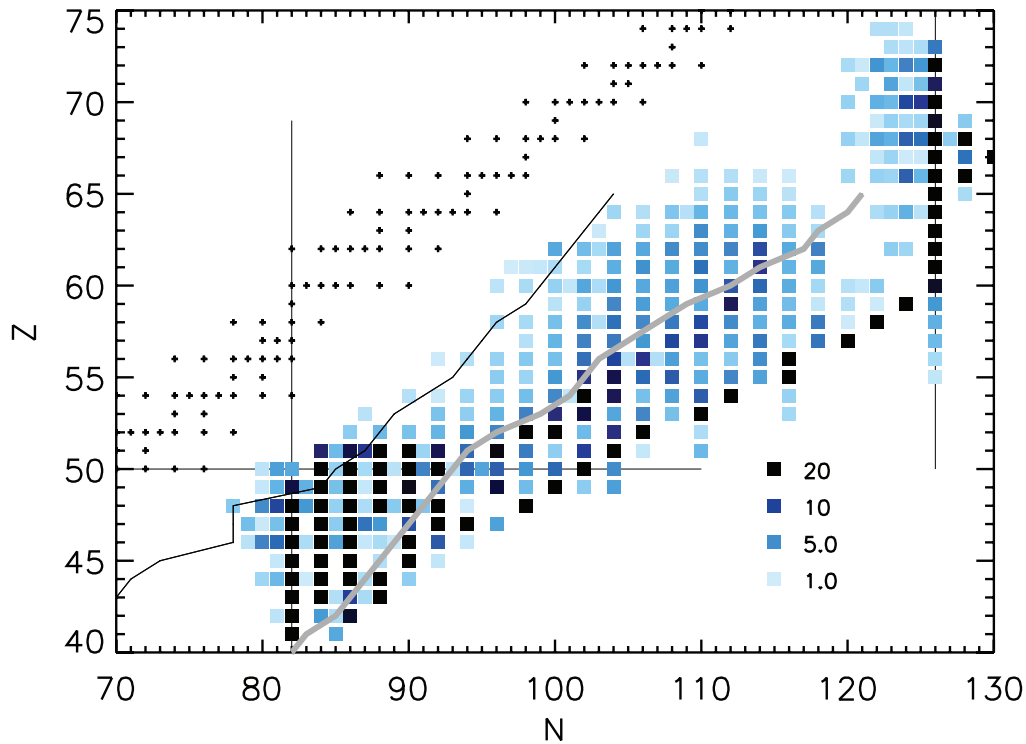


FIG. 9. Compiled results from thirty β -decay sensitivity studies, each starting from a distinct astrophysical trajectory. For each nucleus in the network, the shading indicates the highest sensitivity measure F (Eqn. (5)) obtained. The color scheme is indicated in the lower right hand corner; the darkest squares show nuclei with $F_{max} > 20$. Overlaid are the CARIBU^{32,33} (thin black line) and predicted FRIB³⁴ (thick grey line) accessibility limits (defined as a fission yield greater than 10^{-4}).

final r -process abundance pattern. Such small local changes can be quite important, particularly in the formation of the rare earth peak, the smaller peak around $A \sim 160$ that forms entirely during freezeout.^{7,17} The role of β -decay rates in the formation of the rare earth peak will be the focus of an upcoming study.

An individual β -decay rate can also produce a global change to the final r -process abundance pattern, if the resulting change in nuclear flow alters where the last few free neutrons are consumed. As an example, consider the role of the β -decay rate of ^{140}Te in the cold r -process example simulation. ^{140}Te is not on the r -process path and is only populated early in the freezeout phase, from the β decay of highly abundant ^{140}Sn . It depopulates primarily by β decay as well, as shown in the top panel of Fig. 8, so when the β -decay rate is increased by a factor of 10 it depopulates correspondingly faster. At this time the timescale for neutron captures is roughly that of β decays, so subsequent neutron captures can move material upward in A compared to the baseline simulation. These neutron captures effectively ‘steal’ neutrons from the rest of the nuclear network, as shown in the bottom panel of Fig. 8, producing global changes to the final r -process abundance pattern. This effect is similar to the influence of individual neutron capture rates at late times described in Refs. 26, 31. A decrease to the β -decay rate of ^{140}Te has the opposite effect, such that more material is stuck in ^{140}Te and thus more free neutrons are available for late time captures elsewhere in the network compared to the baseline simulation. Note the effect of decreasing the rate is smaller than increasing it as in the former case the impact is limited by the amount of material flowing into ^{140}Te .³¹

VII. COMPILATION AND CONCLUSIONS

We repeat our sensitivity study procedure for thirty distinct baseline astrophysical scenarios: one merger simulation and the remaining approximately equally split between hot and cold r processes. The results from these thirty sensitivity studies are compiled in Fig. 9, which shows the maximum

TABLE I. Nuclei with β -decay sensitivity measures $F > 5$ from the three example astrophysical scenarios described in Figure 1: a hot wind r process parameterized as in Ref. 19 and 20 with entropy $s/k = 100$, dynamical timescale $\tau_{\text{dyn}} = 80$ ms, and initial electron fraction $Y_e = 0.25$, a cold wind r process from Ref. 21, and a neutron star merger r process from a merger simulation by A. Bauswein and H.-Th. Janka, similar to that from Ref. 24.

Hot r -process			Cold r -process			Merger		
Z	A	F	Z	A	F	Z	A	F
48	132	46.87	48	136	54.36	48	136	84.31
50	138	41.91	46	132	37.14	46	132	52.58
50	140	37.35	47	133	27.85	47	133	39.46
70	196	27.77	44	128	21.49	66	194	24.44
48	130	23.27	49	137	17.35	42	124	18.84
68	194	21.41	50	140	13.72	64	190	17.99
49	135	21.24	42	124	11.86	80	242	17.52
69	195	17.57	52	156	10.66	80	243	16.61
54	156	14.92	66	192	8.713	44	130	15.45
46	128	14.76	49	149	8.318	44	128	14.03
50	136	14.76	65	191	7.969	45	131	13.65
71	197	14.13	68	194	7.931	63	189	13.38
72	198	12.66	51	155	7.814	66	192	11.84
50	134	12.63	64	190	7.766	43	127	10.98
66	192	11.35	63	189	7.334	62	188	9.769
67	193	9.995	43	127	7.056	65	191	8.201
51	141	8.329	50	150	6.821	72	224	8.005
55	159	7.983	69	195	6.442	61	187	7.634
56	160	7.473	67	193	6.293	79	243	7.564
48	134	7.224	70	195	6.175	67	193	6.799
60	174	6.972	58	176	6.169	76	238	6.460
65	191	6.265	62	188	5.911	73	225	6.094
49	131	6.112	59	183	5.710	71	223	6.070
53	153	5.789	61	187	5.200	60	186	5.784
64	190	5.724	41	123	5.057	68	194	5.541
58	168	5.644	56	170	5.046	68	214	5.501
49	133	5.256				50	154	5.089
55	157	5.196						

sensitivity measure F obtained for each nucleus in the main r -process network. Since the different astrophysical scenarios present a variety of possible r -process paths, a wide band of high maximum F measures is seen far from stability, corresponding to this range of paths. Closer to stability, high maximum F measures are found along the β -decay pathways of the closed shell nuclei and also in the rare earth region, as the latter impact the formation of the rare earth peak. Table I shows a subset of those nuclei with F measures greater than 5 for the three example scenarios of hot r process, cold r process, and a merger scenario as described earlier in Figure 1. The overlaid lines from the reach of CARIBU and FRIB are estimates based on fission yields of greater than 10^{-4} . Experimental reach may in fact extend well beyond those lines. The majority of nuclei with high maximum F measures tend to be even- N nuclei. This is encouraging since for the cases very far from stability, outside of the range of the next generation of experimental facilities, even-even nuclei can be more effectively modeled with collective approaches (e.g. QRPA) than their odd counterparts.

While some of the nuclei with the very highest sensitivity measures F lie beyond the presently expected reach of FRIB in this compilation of trajectories, we expect the present and future dedicated radioactive beam facilities within the next decade will make measurements of short-lived neutron-rich nuclei commonplace and provide access to a majority of nuclei important for the r process. Current and future measurements of β -decay lifetimes will help to reduce the large uncertainty that plagues present network calculations allowing us to come within reach of unlocking the longstanding issue of the astrophysical site of the r process.

ACKNOWLEDGMENTS

This work is supported by the National Science Foundation through grant number PHY0758100 and the Joint Institute of Nuclear Astrophysics grant number PHY0822648.

- ¹ E. M. Burbidge, G. R. Burbidge, W. A. Fowler, and F. Hoyle, *Rev. Mod. Phys.* **29**, 547 (1957).
- ² A. G. W. Cameron, Chalk River Rep. **CRL-41** (1957).
- ³ F. Kappeler, R. Gallino, S. Bisterzo, and W. Aoki, *Rev. Mod. Phys.* **83**, 157 (2011).
- ⁴ M. Arnould, S. Goriely, and K. Takahashi, *Phys. Rep.* **450**, 97 (2007).
- ⁵ F.-K. Thielemann *et al.*, *Prog. Part. Nucl. Phys.* **66**, 346 (2011).
- ⁶ A. Arcones and G. Martinez-Pinedo, *Phys. Rev. C* **83**, 045809 (2011).
- ⁷ M. Mumpower, G. C. McLaughlin, and R. Surman, *Phys. Rev. C* **85**, 045801 (2012).
- ⁸ T. Suzuki *et al.*, *Phys. Rev. C* **85**, 015802 (2012).
- ⁹ N. Nishimura *et al.*, *Phys. Rev. C* **85**, 048801 (2012).
- ¹⁰ R. Surman and J. Engel, *Phys. Rev. C* **64**, 035801 (2001).
- ¹¹ T. Rauscher and F.-K. Thielemann, *At. Data Nucl. Data Tables* **75**, 1 (2000).
- ¹² G. Audi, A. H. Wapstra, and C. Thibault, *Nucl. Phys. A* **729**, 337 (2003).
- ¹³ P. Moller, J. R. Nix, W. D. Meyers, and W. J. Swiatecki, *At. Data Nucl. Data Tables* **59**, 185 (1995).
- ¹⁴ P. Moller, B. Pfeiffer, and K.-L. Kratz, *Phys. Rev. C* **67**, 055802 (2003).
- ¹⁵ Evaluated Nuclear Structure Data File, <http://www.nndc.bnl.gov/ensdf/>
- ¹⁶ J. Beun, G. C. McLaughlin, R. Surman, and W. R. Hix, *Phys. Rev. C* **77**, 035804 (2008).
- ¹⁷ R. Surman, J. Engel, J. Bennett, and B. S. Meyer, *Phys. Rev. Lett.* **79**, 1809 (1997).
- ¹⁸ S. Wanajo and Y. Ishimaru, *Nucl. Phys. A* **777**, 676 (2006).
- ¹⁹ B. S. Meyer, *Phys. Rev. C* **89**, 231101 (2002).
- ²⁰ M. Mumpower, G. C. McLaughlin, and R. Surman, *Astrophys. J.* **752**, 117 (2012).
- ²¹ A. Arcones, H.-Th. Janka, and L. Scheck, *Astron. Astrophys.* **467**, 1227 (2007).
- ²² C. Sneden, J. Cowan, and R. Gallino, *Annu. Rev. Astro. Astrophys.* **46**, 241 (2008).
- ²³ I. V. Panov and H.-Th. Janka, *Astron. Astrophys.* **494**, 829 (2009).
- ²⁴ S. Goriely, A. Bauswein, and H.-Th. Janka, *Astrophys. J.* **738**, L32 (2011).
- ²⁵ S. Rosswog, O. Korobkin, A. Arcones, and F.-K. Thielemann, arXiv:1307.2939 (2013).
- ²⁶ R. Surman, J. Beun, G. C. McLaughlin, and W. R. Hix, *Phys. Rev. C* **79**, 045809 (2009).
- ²⁷ S. Brett, I. Bentley, N. Paul, R. Surman, and A. Aprahamian, *E. Phys. J. A* **48**, 184 (2012).
- ²⁸ J. Cass, G. Passucci, R. Surman, A. Aprahamian, *Proceedings of Science NIC-XII* **154** (2012).
- ²⁹ R. Surman, M. Mumpower, J. Cass, and A. Aprahamian, *Proceedings of the Fifth International Conference on Fission and Properties of Neutron-Rich Nuclei* (World Scientific, 2013).
- ³⁰ R. Surman, M. Mumpower, J. Cass, I. Bentley, A. Aprahamian, and G. C. McLaughlin, *Proceedings of the International Nuclear Physics Conference (INPC)* (submitted) arXiv:1309.0059 (2013).
- ³¹ M. Mumpower, G. C. McLaughlin, and R. Surman, *Phys. Rev. C* **86**, 035803 (2012).
- ³² G. Savard and R. Pardo, *Proposal for the ²⁵²Cf source upgrade to the ATLAS facility* (2005).
- ³³ T. R. England and B. F. Rider, *LA-UR-94-3106*, <http://ie.lbl.gov/fission/252Cf.txt>
- ³⁴ O. Tarasov and M. Hausmann, <http://groups.nsl.msu.edu/frib/rates/fribrates.html> (2012).